Cerebral Cortex June 2011;21:1231-1245
doi:10.1093/cercor/bhq199
Advance Access publication November 1, 2010

Developmental Dynamics of Piriform Cortex

Amy A. Sarma[1], Marion B. Richard[1] and Charles A. Greer[1,2,3]

[1]Departments of Neurosurgery, [2]Neurobiology and [3]Interdepartmental Neuroscience Program, Yale University School of Medicine, New Haven, CT 06520, USA

Sarma and Richard contributed equally and share the position of 1st author

Address correspondence to Dr Charles A. Greer, Department of Neurosurgery, Yale University School of Medicine, PO Box 208082, New Haven, CT 06520, USA. Email: charles.greer@yale.edu.

The piriform cortex (PCX) is a trilaminar paleocortex that is of interest for its role in odor coding and as a model for studying general principles of cortical sensory processing. While the structure of the mature PCX has been well characterized, its development is poorly understood. Notably, the kinetics as well as the cellular and morphological basis of the postnatal events that shape the PCX remain unknown. We followed the cellular fates of early- versus late-born cells in layer II of the anterior PCX, with a focus on the molecular maturation of pyramidal cells and the kinetics of their differentiation. We showed that: 1) early-born pyramidal cells differentiate more rapidly than late-born cells and 2) the position of pyramidal cells within the thickness of layer II determines the kinetics of their molecular maturation. We then examined the postnatal development of cortical lamination and showed that the establishment of inhibitory networks in the PCX proceeds through an increase in the density of inhibitory synapses despite a decrease in the number of interneurons. Together, our results provide a more comprehensive view of the postnatal development of the anterior PCX and reveal both similarities and differences in the development of this paleocortex versus the neocortex.

Keywords: inhibition, olfactory, postnatal, pyramidal cells

Introduction

Information processing by cortical networks is critical for normal sensory perception, memory, cognition, and motor responses to the environment. The piriform cortex (PCX) is a paleocortex, one of the architecturally simplest and evolutionarily oldest cortices. It constitutes the third step in the pathway of odor information processing, after the olfactory epithelium and bulb. In contrast to the 6-layered neocortex, the PCX is a 3-layered, or trilaminar, structure. However, like neocortex the PCX has a well-established layer-specific distribution of afferents and efferents (Neville and Haberly 2004). Understanding the organization of the PCX is essential for interpreting the mechanisms underlying odor coding, but the PCX is also an effective model for studying general principles of the formation and function of sensory cortical circuitry.

Afferent input to the PCX is provided by axons of mitral and tufted cells traveling from the olfactory bulb in the lateral olfactory tract (LOT) (Price 1973). The projection neurons of the PCX, superficial and deep pyramidal cells, are located in layers II and III, respectively, and extend apical dendrites into layer I. Pyramidal cell dendrites establish synaptic connections with LOT axons in the superficial portion of layer I (termed layer Ia) and with intracortical association fibers in the deeper aspect of layer I (termed layer Ib) (Haberly and Behan 1983). Semilunar cells are a specific population of neurons located in the superficial-most aspect of layer II that exhibit a dendritic morphology distinct from those of pyramidal cells, as well as specific firing properties and functions (Heimer and Kalil 1978; Haberly and Behan 1983; Wilson et al. 2000; Neville and Haberly 2004; Suzuki and Bekkers 2006). γ-aminobutyric acidergic (GABAergic) interneurons are found in all layers and modulate the activity of pyramidal neurons (Loscher et al. 1998; Luna and Schoppa 2008; Gavrilovici et al. 2010; Luna and Pettit 2010; Suzuki and Bekkers 2010a, 2010b).

While the structure of the adult PCX is well characterized, the development and maturation of this paleocortex is less well understood. Early studies reported both differences and similarities in the development of PCX and neocortex. For example, although the rat PCX lacks an embryonic cortical plate (Schwob and Price 1984a), it develops in an "inside-out" fashion as suggested by injections of [^{3}H]thymidine (Bayer 1986). Many events continue to shape PCX functional connectivity during postnatal development. The inhibitory response to LOT stimulation is not mature until approximately postnatal day (P) 17 (Schwob, Haberly, and Price 1984) and an adult-like spatial distribution of odor-evoked Fos labeling does not emerge until P10 (Illig 2007), suggesting that mature olfactory coding may not develop until the second postnatal week. Rat PCX lamination emerges by the end of the first postnatal week, while synaptogenesis continues over the first couple of weeks (Schwob and Price 1984b; Kunkel et al. 1987; Moriizumi et al. 1995). While it is evident that many crucial events in the development of the anterior piriform cortex (aPC) occur postnatally, the precise kinetics as well as the cellular and morphological basis of these changes remains unidentified. This is particularly true in mice where, although they have emerged as a primary mammalian model for studying the organization of the olfactory system, little is understood regarding the developmental events that shape the organization of PCX.

Here, we first examined the cellular fates of early- versus late-born cells that reside in layer II of the mouse aPC using timed BrdU injections at embryonic days (E) 12, 14, and 16. We focused in particular on the molecular maturation of pyramidal cells and the kinetics of their differentiation. We also examined the postnatal maturation of the aPC neuronal network by analyzing the development of cortical lamination and the emergence of inhibitory mechanisms by quantifying the number of GABAergic interneurons (glutamic acid decarboxylase 67 [GAD67]-green fluorescent protein [GFP]) and the density of inhibitory synapses. Our study extends previous work and provides a more comprehensive understanding of the crucial steps in the postnatal development of the aPC. Our data

on the kinetics of pyramidal cell molecular differentiation and development of the inhibitory network have broad implications for the study of cortical development and the maturation of neuronal networks in sensory cortices.

Materials and Methods

Animals

CD1 (Charles River Laboratories) and heterozygous GAD67-GFP knock-in mice (Tamamaki et al. 2003) were used at P0, P2, P4, P7, P10, P14, P21, P30, and P60 (day of birth = P0). The GAD67-GFP mice were a kind gift from Dr W. Chen (The University of Texas Medical School at Houston). Genotypes of the GAD67-GFP mice were confirmed by polymerase chain reaction. All animal care and use was approved by the Yale University Animal Care and Use Committee.

Tissue Processing

P0, P2, and P4 mice were rapidly decapitated, and brains were removed from the skulls. Brains were immersion fixed in 4% paraformaldehyde (PFA) in phosphate-buffered saline (0.1 M PBS, pH 7.4) at 4 °C overnight. Older postnatal mice (P7 to P60) were deeply anesthetized with pentobarbital and perfused transcardially with PBS containing 1 unit/mL heparin, followed by 4% PFA. Brains were removed from the skulls and postfixed in the same fixative for 2 h. After fixation, the tissue was washed in PBS overnight, cryoprotected in 15% and 30% sucrose in PBS at 4 °C, embedded in OCT compound (Tissue-Tek; Bayer Corporation), and snap frozen in a slurry of dry ice and ethanol. The aPC was serially sectioned at 20 μm in the coronal plane using a Reichart-Jung 2800 Frigocut E cryostat and was distinguished from posterior PCX by the presence of the LOT and demarcated from the neocortex by the rhinal fissure. Sections were thaw mounted onto Superfrost Plus microscope slides (Thermo Fischer Scientific), air-dried, and stored at –20 °C until use.

Immunostaining

Tissue sections were air-dried at room temperature, permeabilized in PBS-T (PBS with 0.3% Triton-X100) for 30 min, and blocked with 5% bovine serum albumin (Sigma Aldrich) in PBS-T at room temperature for 1 h. Primary antibodies were diluted in the blocking solution and applied to sections overnight at 4 °C. Primary and secondary antibodies used are detailed in Table 1. Sections were then rinsed in PBS-T for 10 min and twice in PBS for 10 min before they were incubated with secondary antibodies for 2 h at room temperature. 4',6-diamino-2-phenylindole dihydrochloride (DAPI) (1:1000, Invitrogen) and DRAQ5 (1:1000, Biostatus Ltd) were added to the solution of secondary antibodies when needed to counterstain nuclei. Sections were then rinsed in PBS-T followed by PBS, mounted with Gel/Mount mounting medium (Biomeda), and imaged with an epifluorescence microscope (OlympusBX51) and a laser scanning confocal microscope (Leica TCS SL, Leica Microsystems).

BrdU Birth-Dating Protocol

Animals

Timed-pregnant CD1 females (Charles River Laboratories) received 2 intraperitoneal injections (2 h apart) of 50 mg/kg of BrdU (5-bromo-2-deoxyuridine, Sigma) on E12, E14, or E16 (day of vaginal plug = E0). Two to four pregnant females were injected for each gestational age group, and pups were analyzed at several postnatal ages ranging from P0 to P21.

BrdU Immunostaining

Sections were air-dried at room temperature, treated with 0.025 M HCl for 30 min at 65 °C, cooled at room temperature for 10 min, rinsed in 0.1 M borate buffer (pH 8.5) for 10 min, and finally rinsed in PBS. Immunostaining was then resumed per the protocol described above.

Quantitative Analysis

Unless stated otherwise, analyses were performed on coronal sections through the anteroposterior axis of CD1 mice aPC at P0, P2, P4, P7, P10, P14, P21, P30, and P60. Three sections were quantified and averaged per animal, and 3–5 animals were analyzed per age group for each analysis.

Pyramidal Cell Differentiation in Layer II

Sections were immunostained for T-brain 1 (Tbr1) and neuronal nuclei (NeuN), and confocal images were taken of the ventral-most portion of layer II using a ×40 oil immersion objective. In total, 150–300 $Tbr1^+$ cells in this area were counted per section using ImageJ and classified according to their coexpression of NeuN. In order to analyze the distribution of subpopulations of pyramidal cells within layer II, this layer was divided into 5 equally thick subregions, with bin 1 representing the deepest subregion and bin 5 representing the most superficial region. For each cell population ($Tbr1^+NeuN^-$ or $Tbr1^+NeuN^+$), results were expressed as the percentage of cells located in each bin of the total number of cells in each population (Fig. 2*C–D*). The curve fits that link individual bins are nonlinear regressions (third-order polynomial) and were obtained with GraphPad Prism 4 software (GraphPad software). For statistical analysis, we compared the percentage of cells located in the deep versus superficial halves of layer II (Fig. 2*E–F*). The total numbers of cells counted were 404 and 172 $Tbr1^+NeuN^-$ cells at P0 and P7 respectively, and 1680 and 1653 $Tbr1^+NeuN^+$ cells at P0 and P7.

Laminar Thickness

Sections were immunostained for calretinin, microtubule associated protein 2 (MAP2), and DAPI and imaged using an epifluorescence microscope. Three equidistant lines perpendicular to the surface of the cortical layers were drawn on each image, as shown in Figure 7*B*. The thickness of each layer was measured along these 3 lines using ImageJ and averaged per section.

Laminar Distribution of GAD67-GFP$^+$ Cells

Sections from GAD67-GFP mice were immunostained for calretinin and MAP2 and imaged with an epifluorescence microscope. The $GAD67\text{-}GFP^+$

Table 1
Primary and secondary antibodies

Antigen	Primary antibody		Secondary antibody		
	Source, host (ref)	Dilution	Type	Source	Dilution
Calretinin	Chemicon, mouse IgG1 (ref MAB1568)	1:400	Goat anti-mouse IgG1 Alexa 488 or donkey anti-mouse IgG 555	Invitrogen	1:1000
MAP2	Chemicon, chicken (ref AB5543)	1:500	Goat anti-chicken Alexa 555 or 647	Invitrogen	1:1000
Tbr1	Abcam, rabbit (ref ab31940)	1:1000	Donkey anti-rabbit Alexa 555	Invitrogen	1:1000
NeuN	Chemicon, mouse IgG1 (ref MAB377)	1:700	Goat anti-mouse IgG1 Alexa488 or 647	Invitrogen	1:1000
Gephyrin[a]	Synaptic Systems, mouse IgG1 (clone mAb7a)	1:500	Goat anti-mouse IgG1 Alexa 488	Invitrogen	1:1000
BrdU	Accurate Chemicals, rat (ref OBT0030)	1:300	Goat anti-rat Alexa 488	Invitrogen	1:1000
BLBP	Novus Biologicals, mouse IgG2b (ref NBP-21049)	1:5000	Goat anti-mouse IgG2b Alexa 555	Invitrogen	1:1000

[a]Sections were incubated with the anti-gephyrin primary antibody for 72 h.

cells in the LOT and layer I of each section were counted using ImageJ. Adjacent sections were immunostained for Tbr1, and both the $Tbr1^+$ cells and $GAD67\text{-}GFP^+$ cells in layer II were counted.

Synaptic Density

Sections were immunostained for gephyrin and imaged with a confocal microscope using a ×63 oil immersion objective and 2.5× digital zoom. For each section, 2 randomly sampled, nonoverlapping single plane images were taken from layer Ia, 2 μm below the tissue surface. In order to restrict the analysis to layer Ia, images were taken deep to the LOT at a distance that did not exceed the mean thickness of layer Ia previously measured (see Fig. 7*E*). The intensity of the images was thresholded, and puncta corresponding to synapses were visually identified and counted with ImageJ by an experimenter blind to the age of the animals. For each image, the synaptic density was measured in 3 delineated regions of interest (size 13.4 × 13.4 μm) and averaged (Fig. 9*A*). When nuclei or blood vessels occupied more than one-third of the region of interest selected, the region was excluded from the analysis. The synaptic density reported for each animal is an average of a total of 6 images per animal (3 sections, 2 images each).

BrdU Birth-Dating Protocol

Sections from pups born to BrdU-injected pregnant mice were immunostained for BrdU/Tbr1/NeuN or BrdU/brain lipid binding protein (BLBP)/DRAQ5.

Density of $BrdU^+$ cells. Layer II of P0 and P7 animals injected at E12, E14, and E16 was imaged on an epifluorescence microscope, and the total number of $BrdU^+$ cells in layer II and the area of layer II were quantified with ImageJ.

Subpopulations analysis. Immunostained sections were scanned with a Leica confocal microscope using a ×40 oil immersion objective and 2× digital zoom through the entire thickness of the section, and $BrdU^+$ cells were classified according to their coexpression of the other markers: Tbr1, NeuN, or BLBP (see Figs 1*C* and 5*A*). A minimum of 100 $BrdU^+$ cells were counted per animal from a minimum of 3 sections. The different categories of cells are presented as a percentage of the total number of $BrdU^+$ cells counted (Fig. 3). In an examination solely of immature pyramidal cells present at P7, 100 $Tbr1^+NeuN^-$ pyramidal cells were classified according to the presence or absence of BrdU coexpression in the aPC from pups injected at E12, E14, and E16 (Fig. 4*E*).

To determine the distribution of E12- versus E14-born pyramidal cells within layer II, the ventral-most portion of layer II was imaged with a Leica confocal microscope using the ×40-oil immersion objective on sections from P7 animals immunostained with BrdU, Tbr1, and NeuN. A total of 845 E12-born and 448 E14-born cells were counted and classified according to the molecular markers expressed ($Tbr1^+NeuN^-$ or $Tbr1^+NeuN^+$) and their location within layer II (5 equal subregions as described above for the localization of immature vs. mature pyramidal cells) (Fig. 4*A*–*B*). For statistical analysis, results were expressed as the percentage of cells in each population located in the deep or superficial halves of layer II (Fig. 4*C*–*D*).

Statistical Analyses

Data were graphed, and statistical analyses were processed with GraphPad Prism 4 software (GraphPad software). Results are presented as mean ± standard error of the mean. A one-way analysis of variance (ANOVA) was performed for most of the analyses, followed by Tukey's multiple comparison post hoc tests. We used a 2-way ANOVA when the effect of 2 factors was tested (Figs 1*B* and 5*C*). Unpaired 2-tailed Student *t*-tests were used when only 2 groups were compared. The level of significance was set at $P < 0.05$.

Results

We analyzed the development of the aPC, focusing on the birth-dates of the cell populations in layer II, the kinetics of their molecular differentiation, and the establishment of inhibitory synaptic connections.

Early Versus Late-Born Cells in Layer II

To determine the birth-date of layer II cells, we injected BrdU at E12, E14, or E16 and analyzed the density of $BrdU^+$ cells in layer II at P0 and P7. Layer II was identified as the layer of densely packed cell bodies visualized with DAPI. Cell birth-date had a significant effect on $BrdU^+$ cell density in layer II at P0 and P7 ($F_{2,12} = 92.08$, $P < 0.0001$), with a significantly greater density of cells born at E12 (3951.02 ± 206.95 cells/mm^2 at P0; 2227.79 ± 402.94 cells/mm^2 at P7) than at E14 (705.85 ± 94.77 cells/mm^2 at P0, $P < 0.001$; 1050.84 ± 177.13 cells/mm^2 at P7, $P < 0.01$) or E16 (286.02 ± 90.02 cells/mm^2 at P0, $P < 0.001$; 434.36 ± 76.82 cells/mm^2 at P7, $P < 0.001$) (Fig. 1*B*).

To determine the fate of cells born on these specific embryonic days, aPC sections from P7 pups were immunostained for BrdU, Tbr1 (a marker of postmitotic glutamatergic neurons used to identify pyramidal neurons [Englund et al. 2005; Hevner 2006]), and NeuN (a ubiquitous neuronal marker [Mullen et al. 1992]). Cells were classified as non-neuronal cells ($BrdU^+$), non-pyramidal neurons ($BrdU^+NeuN^+$), or pyramidal neurons ($BrdU^+Tbr1^+$ or $BrdU^+Tbr1^+NeuN^+$) (Fig. 1*C*). Birth-date significantly affected the relative percentages of pyramidal neurons ($F_{2,12} = 99.94$, $P < 0.0001$), non-pyramidal neurons ($F_{2,12} = 120.0$, $P < 0.0001$), and non-neuronal cells ($F_{2,12} = 50.32$, $P < 0.0001$) (Fig. 1*D*–*F*). A greater percentage of cells born at E12 (95.05 ± 0.73%) and E14 (90.03 ± 0.29%) became pyramidal neurons as compared with E16 (43.25 ± 4.89%, $P < 0.001$, Fig. 1*D*). In contrast, a greater percentage of E16-born cells (24.09 ± 1.64%, $P < 0.001$, Fig. 1*E*) became non-pyramidal neurons as compared with E12-born (3.53 ± 0.48%) or E14-born cells (6.75 ± 0.36%). Similarly, a greater percentage of E16-born cells (32.66 ± 4.27%, $P < 0.001$, Fig. 1*F*) became non-neuronal cells as compared with E12-born (1.43 ± 0.29%) or E14-born cells (3.23 ± 0.23%).

In conclusion, most layer II cells of aPC born at earlier stages (E12 and E14) are fated to become pyramidal cells, while half of the cells born later (E16) become either non-pyramidal or non-neuronal cells.

Postnatal Molecular Differentiation of Pyramidal Cells

Pyramidal cells are the projection neurons of the aPC and constitute the main neuronal population present in layer II. We followed the molecular differentiation of pyramidal cells with 2 different markers: Tbr1 and NeuN. Interestingly, some pyramidal cells expressed Tbr1 but not NeuN (Fig. 2*A*, arrows). The percentage of pyramidal cells that were $Tbr1^+NeuN^-$ changed significantly with development ($F_{5,12} = 84.81$, $P < 0.0001$, Fig. 2*B*), decreasing continuously over the first 2 postnatal weeks from 24.31 ± 2.31% at P0 to 9.17 ± 1.03% at P7 ($P < 0.0001$) and ultimately reaching 1.23 ± 0.51% at P14 ($P < 0.01$). Almost none of the $Tbr1^+NeuN^-$ cells persisted after P14, with 0.07 ± 0.07% at P60.

The distribution of the $Tbr1^+NeuN^-$ pyramidal cells within layer II was examined at P0 and P7, the ages at which these cells were most numerous. Layer II was divided into 5 equal subregions, with bins n°1 and n°5 representing the deepest and most superficial subregions of layer II, respectively (Fig. 2*C*–*D*). At P0, $Tbr1^+NeuN^-$ cells were preferentially distributed in the deeper regions (bins 1–4) and avoided the most superficial part

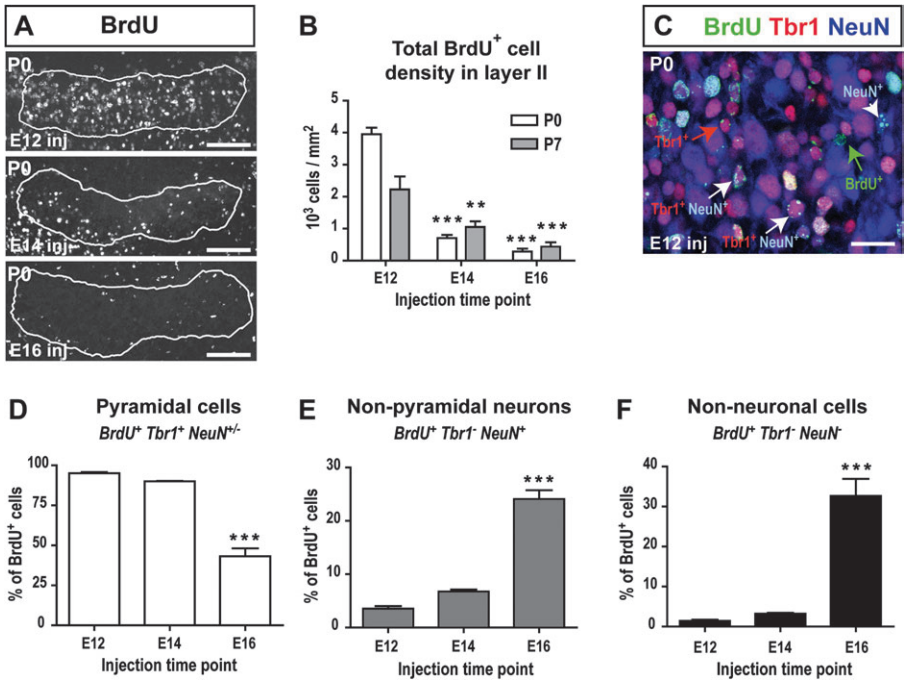

Figure 1. Early versus late-born cells in layer II. (*A*) BrdU-labeled cells in layer II (outlined) at P0. (*B*) Density of $BrdU^+$ cells in layer II at P0 and P7. $n = 3$ animals per injection time point and per age. (*C*) Examples of the different cell subpopulations ($BrdU^+$, $BrdU^+/NeuN^+$, $BrdU^+/Tbr1^+$, or $BrdU^+/Tbr1^+/NeuN^+$) identified on an E12-injected P0 section. (*D*) Percent of BrdU-labeled pyramidal neurons ($BrdU^+/Tbr1^+$ or $BrdU^+/Tbr1^+/NeuN^+$) at P7. (*E*) Percent of BrdU-labeled non-pyramidal neurons ($BrdU^+/NeuN^+$) at P7. (*F*) Percent of BrdU-labeled non-neuronal cells ($BrdU^+$) at P7. Asterisks signify that E12 was significantly different from E14 and E16 in B (2-way ANOVA followed by Tukey's post hoc tests) and that E16 was significantly different from E12 and E14 in (*D–F*) (one-way ANOVA followed by Tukey's post hoc tests). $n = 5$ animals per injection time point. $^{**}P < 0.01$; $^{***}P < 0.001$. Scale bars = 100 μm in *A*, 20 μm in *B*.

of layer II (bin 5), while $Tbr1^+NeuN^+$ cells were uniformly distributed across all bins (Fig. 2*C*). The preferential distribution of $Tbr1^+NeuN^-$ cells in the deeper part of layer II was more pronounced at P7 (Fig. 2*D*). When the percentages of cells located in the deeper and superficial halves of layer II were compared, significantly more $Tbr1^+NeuN^-$ pyramidal cells were located in the deeper half of layer II at both P0 and P7 ($P = 0.0442$ at P0 and $P = 0.0057$ at P7; Fig. 2*E*1,*F*1). While the $Tbr1^+NeuN^+$ population was evenly distributed at P0 (Fig. 2*E*2), a significantly greater percentage of $Tbr1^+NeuN^+$ cells were located in the superficial half of layer II at P7 ($P = 0.0014$; Fig. 2*F*2).

To test the hypothesis that the $Tbr1^+NeuN^-$ cells are immature pyramidal cells that will eventually express NeuN and study the kinetics of this maturation sequence, we combined cell birth-dating by BrdU injection (E12, E14, E16) with markers of pyramidal cell maturation (Tbr1 and NeuN). BrdU-labeled layer II cells were classified as $BrdU^+$, $BrdU^+NeuN^+$, $BrdU^+Tbr1^+$, or $BrdU^+Tbr1^+NeuN^+$ for each postnatal age, as shown in Figure 1*C*.

A small percentage of E12-born cells were $BrdU^+$ (2.41 ± 0.47%, Fig. 3*A*1) or $BrdU^+Tbr1^+$ (4.51 ± 2.11%, Fig. 3*A*2) at P0. These percentages did not change between P0 and P7 (Fig. 3*A*1–*A*2). The majority of E12-born cells were $BrdU^+Tbr1^+NeuN^+$ at P0 (86.36 ± 2.11%, Fig. 3*A*3), and this percentage increased over the first postnatal week, comprising 91.67 ± 0.85% of BrdU-labeled cells by P7 ($P = 0.0482$).

A small percentage of E14-born cells were $BrdU^+$ (18.19 ± 5.20%, Fig. 3*B*1) or $BrdU^+Tbr1^+$ (7.6 ± 1.28%, Fig. 3*B*2) at P0, and these 2 percentages changed significantly with postnatal development ($F_{2,12} = 7.841$, $P = 0.0066$, Fig. 3*B*1 and $F_{2,12} = 6.219$, $P = 0.0140$, Fig. 3*B*2). The percentage of $BrdU^+$ cells dropped during the first postnatal week from 18.19 ± 5.20% at P0 to 3.23 ± 0.23% at P7 ($P < 0.05$), after which this population remained stable. The percentage of $BrdU^+Tbr1^+$ cells declined progressively over the first 2 postnatal weeks, decreasing significantly from 7.6 ± 1.28% at P0 to 2.41 ± 0.62% by P14 ($P < 0.05$). The majority of E14-born cells were $BrdU^+Tbr1^+NeuN^+$ at P0 (50.10 ± 7.07%, Fig. 3*B*3), and this percentage changed significantly with development ($F_{2,12} = 24.03$, $P < 0.0001$); the percentage of $BrdU^+Tbr1^+NeuN^+$ cells increased from P0 to P7 ($P < 0.001$) and stabilized thereafter, representing 86.44 ± 1.66% of E14-born cells by P14.

In contrast to E12 and E14-born cells, the majority of E16-born cells were $BrdU^+$ (69.25 ± 8.23%, Fig. 3*C*1) at P0. The percentage of $BrdU^+$ cells changed significantly during postnatal development ($F_{6,24} = 12.38$, $P < 0.0001$, Fig. 3*C*1); there was a reduction over the first postnatal week, with a notable decrease from P0–P2 to P7 ($P < 0.05$). After P7, the $BrdU^+$ population remained stable, representing 18.54 ± 3.93% of E16-born cells at P21. The percentage of $BrdU^+Tbr1^+$ cells also changed developmentally ($F_{6,24} = 10.77$, $P < 0.0001$, Fig. 3*C*2). This population increased over the first postnatal week and peaked at P7, representing 28.14 ± 3.85% of the E16-born cells. Over the second postnatal week, the $BrdU^+Tbr1^+$ cell population declined, with a significant decrease between P7 and P14–P21 ($P < 0.05$) and ultimately represented a relatively small percentage of E16-born cells by P21 (5.32 ± 0.52%). Finally, the percentage of $BrdU^+Tbr1^+NeuN^+$ cells also changed during postnatal development ($F_{6,24} = 29.16$, $P < 0.001$, Fig. 3*C*3). This population gradually increased over the first and second postnatal weeks, with a significant increase

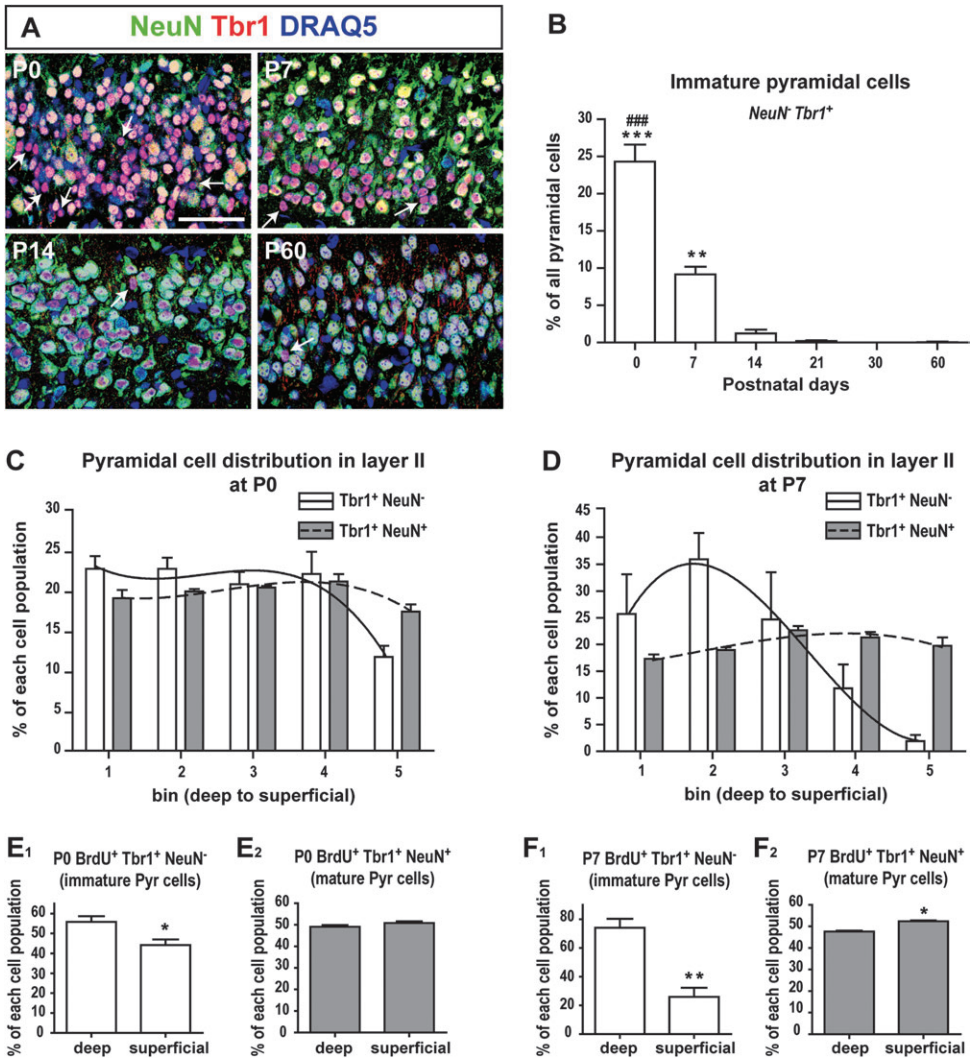

Figure 2. Postnatal molecular differentiation of pyramidal cells. (*A*) Some pyramidal cells (arrows) expressed Tbr1 but not NeuN in layer II. (*B*) Decrease in the percentage of NeuN$^-$ pyramidal cells during postnatal development. Asterisks (*) denote groups significantly different from P14–P60 while the pound (#) sign signifies a significant difference from P7 (one-way ANOVA followed by Tukey's post hoc tests). (*C–D*) Distribution of immature (Tbr1$^+$NeuN$^-$) and mature (Tbr1$^+$NeuN$^+$) pyramidal cells within the thickness layer II at P0 (*C*) and P7 (*D*). Layer II was divided into 5 equally thick subregions (called bins), and bin n°1 represents the deepest part of layer II. (*E–F*) Distribution of Tbr1$^+$NeuN$^-$ (E1 and F1) and Tbr1$^+$NeuN$^+$ (E2 and F2) pyramidal (Pyr) cells in the deep versus superficial halves of layer II at P0 (*E*) and P7 (*F*). $n = 3$ animals per age. $^*P < 0.05$; $^{**}P < 0.01$; $^{***}P < 0.001$; $\#\#\#P < 0.001$. Unpaired 2-tailed Student *t*-tests. Scale bar = 50μm.

from 1.40 ± 0.41% at P0 to 15.11 ± 1.90% at P7 ($P < 0.01$) and 39.77 ± 6.13% at P14 ($P < 0.001$). After P14, the BrdU$^+$Tbr1$^+$NeuN$^+$ cell population reached a plateau, representing 43.08 ± 13.66% of E16-born cells at P21.

Collectively, these results show that the molecular differentiation of pyramidal cells involves the successive expression of Tbr1 and NeuN. Interestingly, the kinetics of this differentiation seemingly depends on the birth-date of the pyramidal cells, with early-born cells (E12 and E14) differentiating more rapidly than late-born E16 cells (see Fig. 10 and Discussion).

Having demonstrated that cell birth-date affects the kinetics of pyramidal cell maturation, we next asked if it also determined the position of pyramidal cells within layer II, as suggested by [^{3}H]thymidine labeling (Bayer 1986). Therefore, we classified E12- and E14-born layer II pyramidal cells based on their molecular phenotype and then analyzed their distribution at P7. These embryonic ages were chosen because significantly more pyramidal cells were born on these days than at E16 (Fig. 1*D*). While E12-born pyramidal cells (Tbr1$^+$NeuN$^{+/-}$) were evenly distributed throughout the thickness of layer II at P7 (Fig. 4*A*,*C*1), a greater percentage of E14-born pyramidal cells tended to be located in the deeper half of layer II (Fig. 4*B*,*D*1; $P = 0.0525$). These results suggest that cell birth-date markedly affects the position of pyramidal cells in layer II, with early-born (E12) cells settling homogeneously throughout layer II, and later-born (E14) cells settling in the deeper part of layer II. When the distribution of immature (Tbr1$^+$NeuN$^-$) versus mature pyramidal cells (Tbr1$^+$NeuN$^+$) born at E12 and E14 were analyzed separately at P7, we found that immature pyramidal cells were significantly more numerous in the deeper half of layer II (Fig. 4*C*2,*D*2, $P < 0.0001$ for E12 and $P = 0.0107$ for E14), and mature pyramidal cells were distributed uniformly in layer II (Fig. 4*C*3,*D*3) whether they were born at E12 or E14. These results demonstrate that within a population of pyramidal cells born on the same day, cells that settle in the deeper portion of

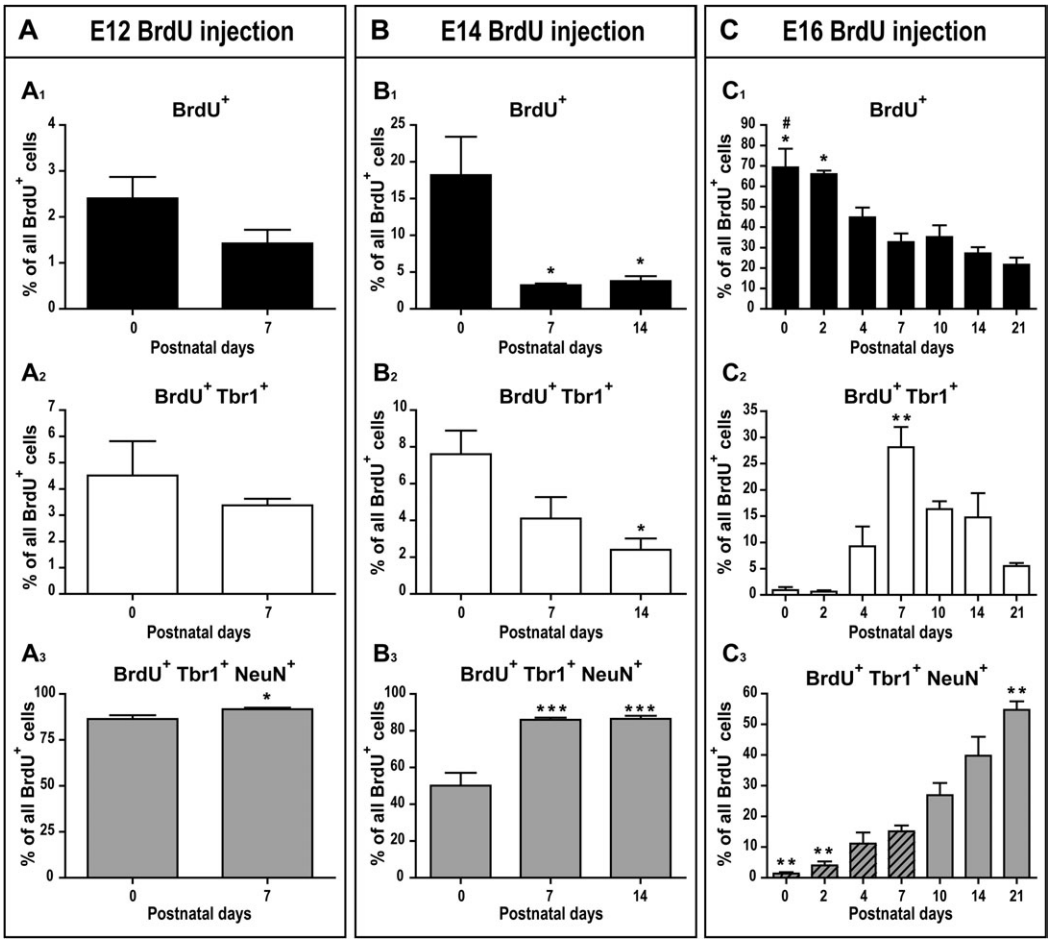

Figure 3. Postnatal molecular differentiation of layer II pyramidal cells according to their birth-date. Postnatal changes in the percentages of E12- (*A*), E14- (*B*), and E16-born cells (*C*) classified as $BrdU^+$ (*A*1, *B*1, *C*1), $BrdU^+/Tbr1^+$ (*A*2, *B*2, *C*2), or $BrdU^+/Tbr1^+/NeuN^+$ (*A*3, *B*3, *C*3). Asterisks signify a significant difference between marked groups and P0 (*A*1–*B*3). Unpaired 2-tailed Student *t*-tests in (*A*) and one-way ANOVA followed by Tuckey's post hoc tests in (*B*) and (*C*). (*C*1) Asterisks signify a significant difference between marked groups and P7–P21, while the pound sign denotes a significant difference between the marked group and P4. (*C*2) Asterisks signify that P7 was significantly different from P0–P4 and P14–P21. Not all significant post hoc tests are shown. (*C*3) Striped groups denote those that were significantly different from P14–P21 ($P < 0.05$) and asterisks signify a significant difference between the marked groups and P10. $n = 3$–5 animals per age for each injection time point. $^*P < 0.05$; $^{**}P < 0.01$; $^{***}P < 0.001$.

layer II are still immature at P7, while cells in the superficial layer II are already mature, strongly suggesting that positioning within layer II affects the kinetics of pyramidal cell maturation. In addition, among the $Tbr1^+NeuN^-$ cells detected at P7, the percentages of cells born at E12, E14, and E16 were equivalent (28.18 ± 4.19%, 27.31 ± 3.90%, and 23.39 ± 5.90%, respectively, Fig. 4*E*), further demonstrating that even though there may be a preference for late-born pyramidal cells to settle deeper in layer II, a positional effect delays the maturation of pyramidal cells, irrespective of birth-date.

Postnatal Differentiation of Radial Glia Precursors

We hypothesized that some of the $BrdU^+$ cells that did not coexpress Tbr1 or NeuN at early postnatal ages ($BrdU^+Tbr1^-NeuN^-$ cells, abbreviated as $BrdU^+$) were radial glia precursors. To confirm this phenotype, we stained aPC sections for BLBP, a marker expressed ubiquitously by radial glia postnatally (Feng et al. 1994; Hartfuss et al. 2001). We conducted this analysis on E16-injected pups because this group had the highest percentage of $BrdU^+$ cells during the first postnatal week (see Fig. 3). BrdU-labeled cells were categorized according to their coexpression of BLBP as shown in Figure 5*A*. The percentage of $BrdU^+BLBP^+$ cells changed significantly during development ($F_{5,15} = 10.48$, $P = 0.0002$, Fig. 5*B*). This population decreased between P0 and P2 ($P < 0.05$) from 64.63 ± 2.60% to 40.03 ± 6.51% and remained stable thereafter. We then compared the percent of $BrdU^+Tbr1^-NeuN^-$ cells (Fig. 3*C*1) from the neuronal marker analysis to the $BrdU^+BLBP^+$ cells from this analysis, with the hypothesis that if they indeed represent a single cell population, these percentages would be identical at each postnatal age. A 2-way ANOVA showed a significant effect of age and cell marker ($F_{5,37} = 17.79$, $P < 0.0001$ and $F_{1,37} = 10.31$, $P = 0.0027$, Fig. 5*C*). At all the ages excluding P2, there was no difference between the $BrdU^+Tbr1^-NeuN^-$ population and the $BrdU^+BLBP^+$ population (e.g., 69.25 ± 8.23% for $BrdU^+Tbr1^-NeuN^-$ cells vs. 64.63 ± 2.60% for $BrdU^+BLBP^+$ cells at P0; 27.21 ± 2.65% vs. 29.85 ± 4.65% at P14). However, at P2, the percentage of $BrdU^+BLBP^+$ cells (40.03 ± 3.76%) was significantly lower than that of the $BrdU^+Tbr1^-NeuN^-$ cells (65.93 ± 1.59%, $P < 0.01$), indicating that the percentage of $BrdU^+BLBP^+$ cells decreased earlier than the percentage of $BrdU^+Tbr1^-NeuN^-$ cells. This is consistent with our hypothesis that the $BrdU^+Tbr1^-NeuN^-$ cells are radial glia precursors, some

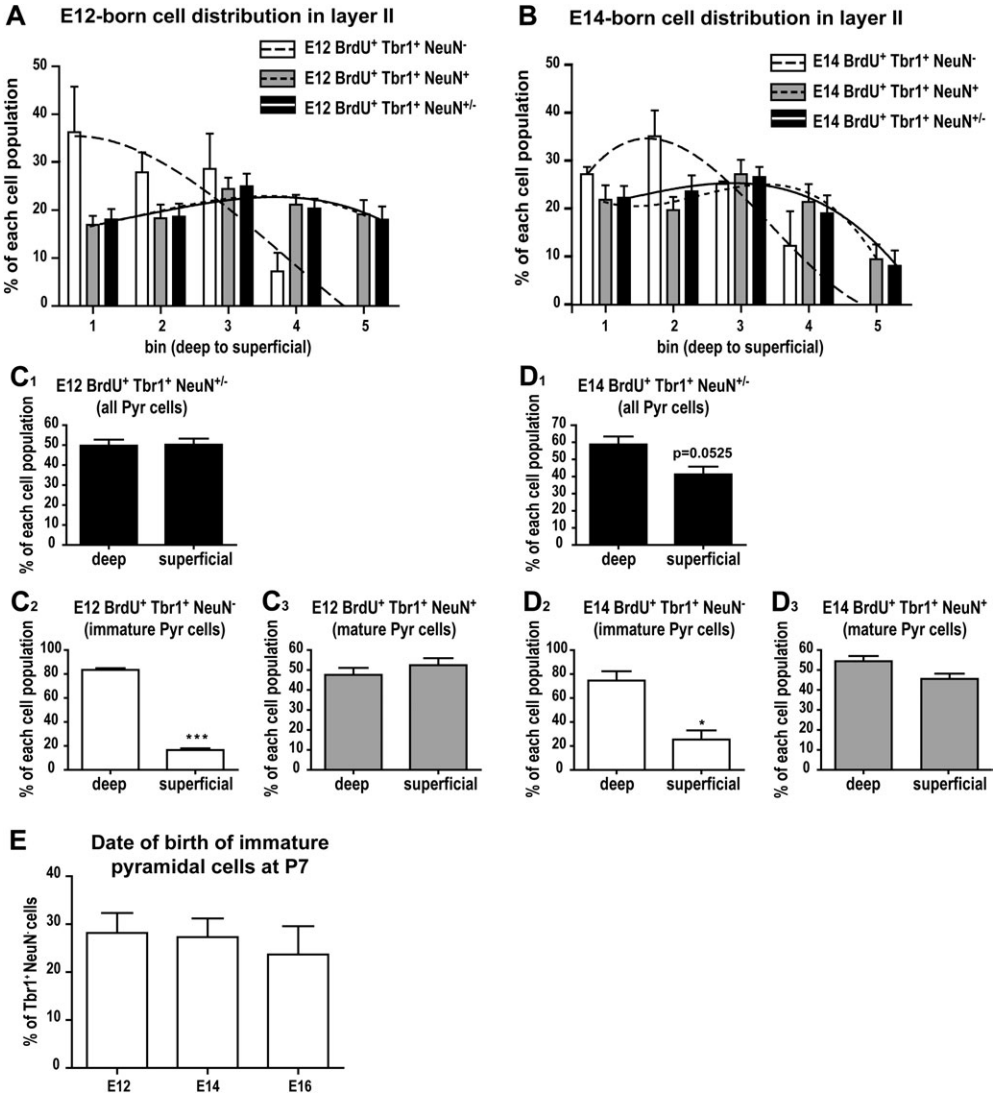

Figure 4. Pyramidal cell distribution in layer II based on birth-date. Distribution of E12- (*A*) and E14- (*B*) born pyramidal cells within the thickness of layer II at P7. Layer II was divided into 5 equally thick subregions (called bins) and bin n°1 represents the deepest portion of layer II. (*C–D*) Distribution of E12- and E14-born pyramidal (Pyr) cells within the deep and superficial halves of layer II (unpaired 2-tailed Student *t*-tests): cell populations analyzed are all pyramidal cells (*C*1, *D*1), immature $Tbr1^{+}NeuN^{-}$ (*C*2, *D*2), and mature $Tbr1^{+}NeuN^{+}$ pyramidal cells (*C*3, *D*3). (*E*) Relative contribution of each birth-date (E12, E14, E16) to the population of immature $Tbr1^{+}NeuN^{-}$ pyramidal cells present at P7 (one-way ANOVA followed by Tuckey's post hoc tests). $n = 3$ animals per injection time point. $^{*}P < 0.05$; $^{***}P < 0.001$.

of which transition from a radial glial phenotype to a neuronal phenotype, down-regulating BLBP before expressing Tbr1.

Postnatal Maturation of Interneurons in Layer II

Interneurons were identified by the expression of NeuN but not Tbr1 ($BrdU^{+}Tbr1^{-}NeuN^{+}$, abbreviated $BrdU^{+}NeuN^{+}$). The $BrdU^{+}NeuN^{+}$ population represented a minority of E12-born cells and significantly decreased from 6.72 ± 1.06% at P0 to 3.53 ± 0.48% at P7 (Fig. 6*A*, $P = 0.0251$). In contrast, a relatively high proportion of E14- and E16-born cells were $BrdU^{+}NeuN^{+}$ at P0 (24.10 ± 3.32% for E14-born cells and 28.43 ± 9.67% for E16-born cells, Fig. 6*B–C*). The percentage of $BrdU^{+}NeuN^{+}$ cells born on E14 significantly changed developmentally ($F_{2,12} = 23.25$, $P < 0.0001$, Fig. 6*B*), decreasing over the first postnatal week from 24.10 ± 3.32% at P0 to 6.75 ± 0.36% at P7 ($P < 0.001$). However, the percentage of $BrdU^{+}NeuN^{+}$ cells born on E16 remained stable during postnatal development (Fig. 6*C*).

Postnatal Development of the Laminar Organization of the aPC

The development of the aPC involves the increased arborization of the pyramidal cell dendrites and establishment of the synaptic network. This can be analyzed through the study of the laminar organization of the developing aPC. To do so, we used 3 markers—calretinin, MAP2, and DAPI—which enabled us to delineate the aPC layers from P0 to P60. MAP2 identified dendrites (Caceres et al. 1983; Bernhardt and Matus 1984) that span the entirety of layer I. Calretinin labeled mitral cell axons (Bulfone et al. 1998), which comprise the LOT and extend through layer Ia, where they synapse with dendrites of pyramidal cells and interneurons (Price 1973; Haberly and Behan 1983). Thus, the LOT was identified as the area that stained only for calretinin, and layer Ia as the area where calretinin and MAP2 were both detected (Fig. 7*A–B*). Since LOT axons do not extend further into layer Ib (Schwob and Price 1984b), layer Ib was defined as the region that stained only for

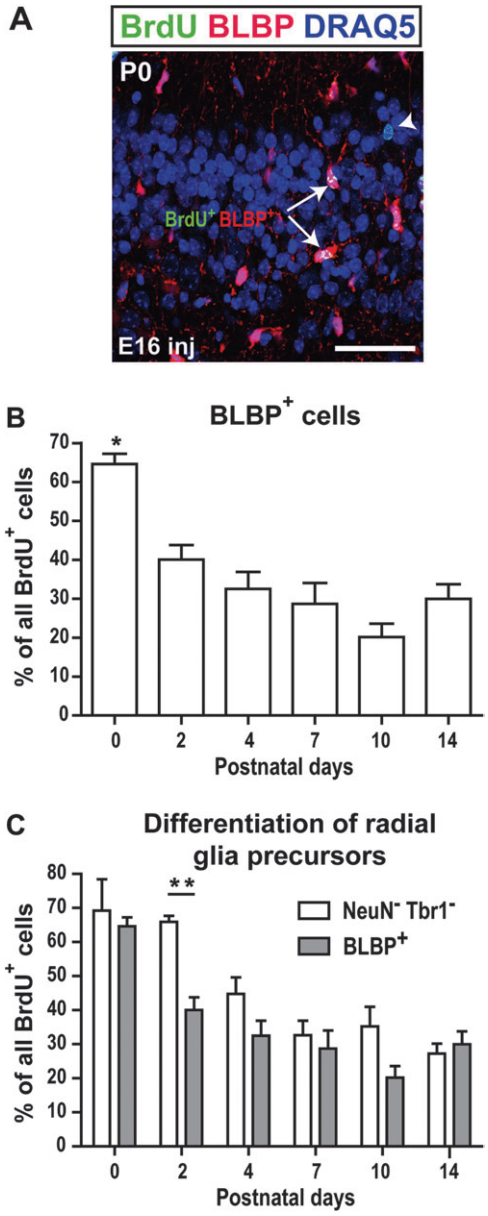

Figure 5. Postnatal differentiation of radial glia precursors. (*A*) Example of the 2 cell subpopulations ($BrdU^+/BLBP^+$ arrow and $BrdU^+/BLBP^-$ arrowhead) identified on an E16-injected P0 section. (*B*) Postnatal changes in the percentage of $BrdU^+/BLBP^+$ cells. Asterisks signify a significant difference between P0 and P2–P14 (one-way ANOVA followed by Tuckey's post hoc tests). (*C*) Comparison of the percentage of the $BrdU^+/NeuN^-/Tbr1^-$ and $BrdU^+/BLBP^+$ cell populations. Asterisks denote a significant difference between these 2 populations at P2 (2-way ANOVA followed by Tuckey's post hoc tests). Scale bar = 50 μm. n = 3–5 animals per age. $^*P < 0.05$; $^{**}P < 0.01$.

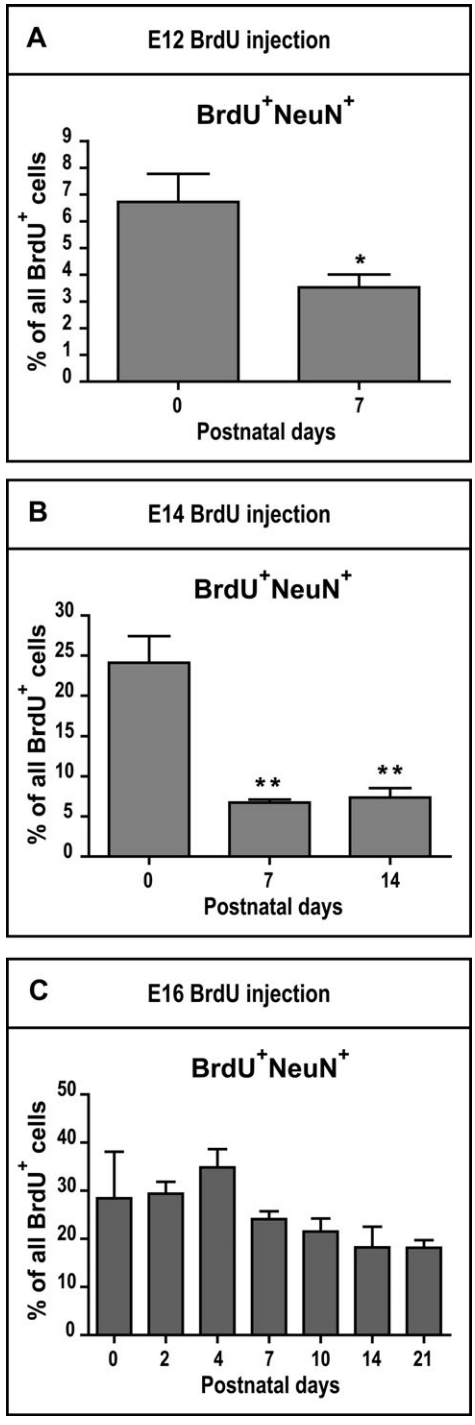

Figure 6. Postnatal maturation of layer II interneurons. Postnatal changes in the percentages of E12- (*A*), E14- (*B*), and E16-born (*C*) $BrdU^+/NeuN^+$ cells. Asterisks signify a significant difference between the marked group and P0 (*A*–*B*). Unpaired 2-tailed Student *t*-tests in *A* and one-way ANOVA followed by Tuckey's post hoc tests in *B* and *C*. n = 3–5 animals per age. $^*P < 0.05$; $^{**}P < 0.01$.

MAP2. Layer II was identified as the layer of densely packed cell bodies visualized with DAPI. Since layer III lacks a distinct anatomical boundary at its medial aspect, we restricted our analysis to the LOT, layer I, and layer II. The thickness of the aPC increased during postnatal development (from P0 to P60), as shown in Figure 7*A*. The total thickness of the aPC (from the LOT through layer II) more than doubled from 213.72 ± 15.32 μm at P0 to 494.97 ± 32.76 μm at P60 (data not shown, $F_{7,19}$ = 13.56, $P < 0.0001$). We analyzed the evolution of each aPC layer independently and concordant with the increase in total cortical thickness, all the component layers of the aPC increased in thickness between P0 and P60 (Fig. 7*C*–*G*). The thickness of the LOT changed significantly during development from 60.82 ± 0.45 μm at P0 to 161.35 ± 15.76 μm at P60 ($F_{7,19}$ = 18.76, $P < 0.0001$, Fig. 7*C*). This increase occurred in 2 steps: an initial increase after the first postnatal week, with a significant

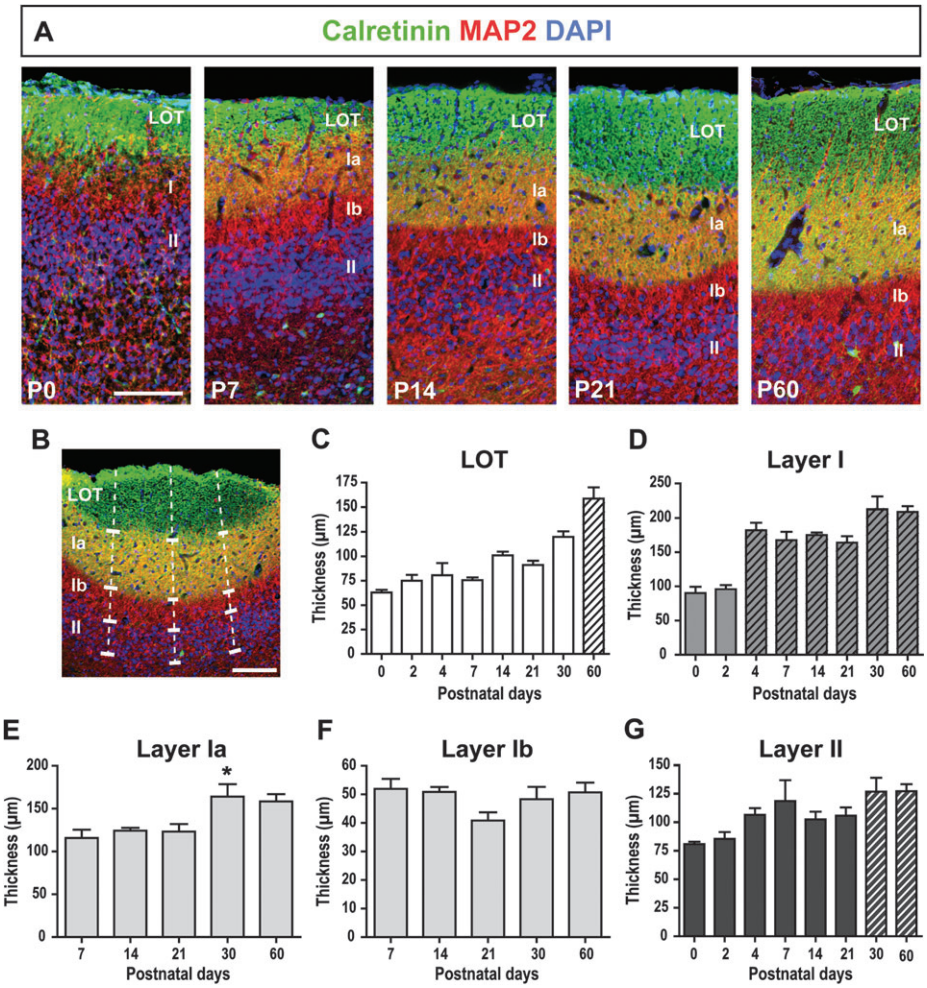

Figure 7. Postnatal development of the laminar organization of the aPC. (*A*) Development of the laminar organization of the aPC from P0 to P60 visualized by immunostaining for Calretinin, MAP2, and DAPI. (*B*) Schematic of the method used to measure the thickness of each cortical layer using 3 lines perpendicular to the cortical surface. (*C*) Postnatal changes in the LOT thickness. The asterisks (*) denote groups significantly different from P0 and the pound sign (#) signifies a significant difference from P2 to P7. P60 (striped) was significantly different from all the other ages ($P < 0.05$). (*D*) Postnatal changes in the thickness of layer I. Striped groups highlight those significantly different from P0 and P2 ($P < 0.01$). (*E*) Postnatal changes in the thickness of layer Ia. The asterisk denotes a significant difference from P7 ($P < 0.05$). (*F*) Postnatal stability of the thickness of layer Ib. (*G*) Postnatal changes in the thickness of layer II. P30 and P60 (striped) were significantly different from P0 ($P < 0.05$). One-way ANOVA followed by Tuckey's post hoc tests (*C*–*G*). Scale bars = 100 μm in *A* and *B*. n = 3–4 animals per age. *$P < 0.05$.

difference between P7 and P30 ($P < 0.05$), followed by a second increase between P30 and P60 ($P < 0.05$).

The thickness of layer I also changed significantly from 76.40 ± 12.86 μm at P0 to 204.89 ± 8.97 μm at P60 ($F_{7,19}$ = 15.99, $P < 0.0001$, Fig. 7*D*). This increase occurred between P2 and P4 ($P < 0.01$), after which the thickness of layer I remained stable. However, the subdivision of layer I into layers Ia and Ib did not emerge until P7, as shown in Figure 7*A*. From P7 onward, the thickness of layer Ia increased significantly from 127.38 ± 21.27 μm at P7 to 164.11 ± 14.4 μm at P30 ($F_{7,19}$ = 15.99, P = 0.0135, Fig. 7*E*), while the thickness of layer Ib remained stable (Fig. 7*F*). Finally, the thickness of layer II significantly increased from 76.50 ± 2.90 μm at P0 to 128.72 ± 8.45 μm at P60 ($F_{7,19}$ = 3.479, P = 0.0143, Fig. 7*G*). This increase occurred more gradually, with a significant difference emerging between P0 and P30–P60 ($P < 0.05$).

Postnatal Changes in the Interneuron Population

To examine developmental changes in the number and distribution of interneurons in the aPC, we used a GAD67-GFP mouse line (Tamamaki et al. 2003) to identify GABAergic interneurons and quantified the GAD67-GFP$^+$ cells in the LOT, layer I, and layer II. Sections were also stained for calretinin and MAP2 to delineate the layers, as described in the previous section (Fig. 8*A*).

The number of GAD67-GFP$^+$ cells in the LOT ($F_{7,17}$ = 7.682, P = 0.0003, Fig. 8*B*) and layer I ($F_{7,17}$ = 4.440, P = 0.0057, Fig. 8*C*) changed significantly with development. The number of GAD67-GFP$^+$ cells in the LOT initially increased between P0 and P2 ($P < 0.05$), reaching a maximum of 14.33 ± 4.68 cells per section at P2 (Fig. 8*B*). The number of interneurons then decreased significantly between P2 and P7 to 4.44 ± 0.48 cells per section ($P < 0.05$). By the second postnatal week, the GAD67-GFP$^+$ population had stabilized in the LOT, reaching 2.22 ± 0.11 cells per section at P60. In layer I, the number of GAD67-GFP$^+$ cells peaked at P2 (47.11 ± 7.14 cells per section), after which it decreased to 20.00 ± 4.98 cells per section by P14 ($P < 0.05$, Fig. 8*C*). By the second postnatal week, the number of interneurons had stabilized and reached 15.11 ± 4.04 cells per section at P60. Layer II contained the highest

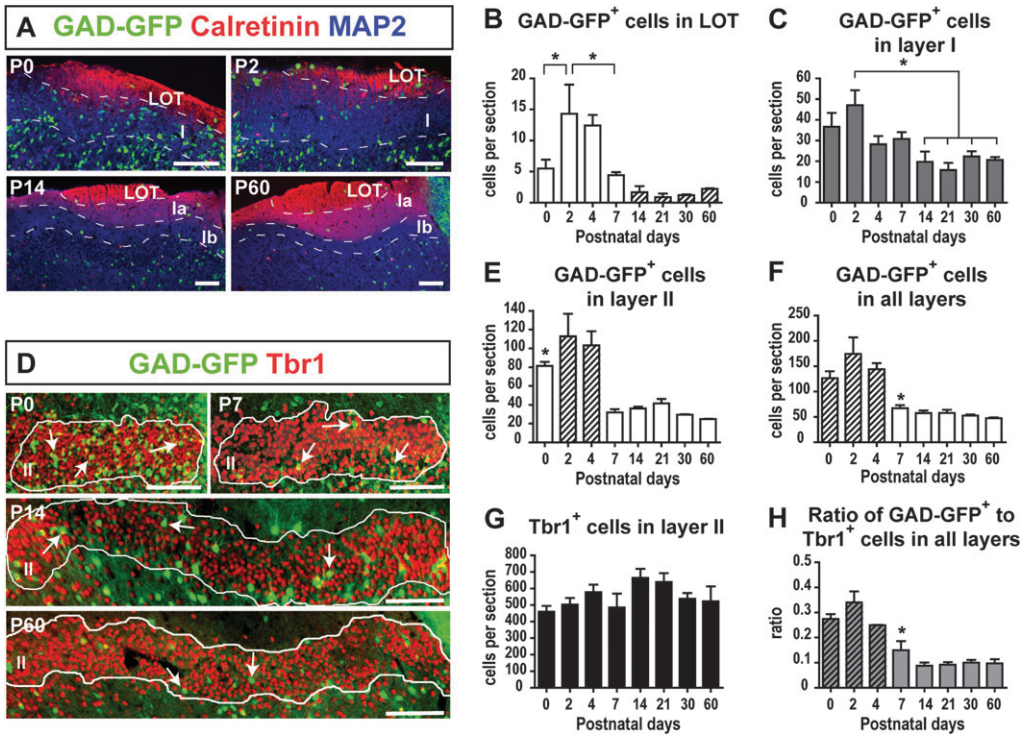

Figure 8. Developmental distribution of interneurons in the aPC. (*A*) Postnatal development of the laminar distribution of GAD67-GFP$^+$ cells in the LOT and layer I. (*B*) Number of GAD67-GFP$^+$ cells in the LOT per section. Striped groups denote those significantly different from P2 and P4 ($P < 0.05$). (*C*) Number of GAD67-GFP$^+$ cells in layer I per section. (*D*) GAD67-GFP$^+$ interneurons (arrows) and Tbr1$^+$ pyramidal cells in layer II (outlined) from P0 to P60. (*E*) Number of GAD67-GFP$^+$ cells in layer II per section. The asterisk indicates that P0 was significantly different from P30 to P60. P2 and P4 (striped) were significantly different from P7 to P60 ($P < 0.05$). (*F*) Number of GAD67-GFP$^+$ cells in all the aPC layers (LOT through layer II). Striped groups denote those significantly different from P14 to P60 ($P < 0.05$) and the asterisk signifies a significant difference from P2 to P4. (*G*) Number of Tbr1$^+$ cells in layer II per section. (*H*) Ratio of GAD67-GFP$^+$ interneurons to Tbr1$^+$ cells in the entire aPC. Stripes denote groups significantly different from P14 to P60 ($P < 0.01$) and the asterisk denotes a significant difference from P0 to P2. Scale bars = 100 μm in *A* and *D*. $n = 3$ animals per age. One-way ANOVA followed by Tuckey's post hoc tests in *B–C* and *E–H*. *$P < 0.05$.

number of interneurons, and this number also changed significantly with development ($F_{7,16} = 11.96$, $P < 0.0001$, Fig. 8*D–E*). The number of GAD67-GFP$^+$ cells peaked at P2 with 112.78 ± 24.11 cells per section and significantly declined between P4 and P7 to 31.89 ± 3.38 cells per section ($P < 0.01$). It remained stable after the first postnatal week, with 20.67 ± 1.35 cells per section in layer II at P60.

In summary, the total number of GAD67-GFP$^+$ cells in all the layers examined changed significantly with development ($F_{7,16} = 12.97$, $P < 0.0001$, Fig. 8*F*), peaking at P2 with 174.22 ± 32.63 cells per section, and then decreasing significantly between P4 and P7 ($P < 0.05$). After the first postnatal week, the total number of GAD67-GFP$^+$ cells stabilized, with 47.67 ± 1.35 cells per section at P60.

To quantify pyramidal cells in layer II, adjacent aPC sections were stained for Tbr1 (Fig. 8*D*). In contrast to the interneurons, the Tbr1$^+$ pyramidal cell population remained stable in layer II throughout development (Fig. 8*G*). Consequently, the ratio of GAD67-GFP$^+$ interneurons to Tbr1$^+$ pyramidal cells in the aPC changed developmentally ($F_{7,16} = 18.59$, $P < 0.0001$, Fig. 8*H*). This ratio decreased significantly during the first postnatal week from 0.34 ± 0.04 at P2 to 0.15 ± 0.04 at P7 ($P < 0.001$) and was further reduced over the second postnatal week, with a ratio at P14 (0.09 ± 0.01) that was significantly lower than at P4 ($P < 0.01$). After P14, the ratio of GAD67-GFP$^+$ to Tbr1$^+$ cells remained stable, with a ratio of 0.10 ± 0.02 at P60 (1 interneuron: 10 pyramidal cells).

In conclusion, a significant reduction in the ratio of interneurons to pyramidal cells occurred in the developing aPC during the first and second postnatal weeks.

Postnatal Changes in Inhibitory Synapse Density

Electrophysiological analyses suggest that cortical inhibition increases over the first 3 postnatal weeks in rat (Schwob, Haberly, and Price 1984). We hypothesized that although we found a developmental decrease in the number of GAD67-GFP$^+$ cells in the aPC, the density of inhibitory synapses may nonetheless increase. To test this hypothesis, we examined the postnatal changes in the density of inhibitory synapses in layer Ia. We identified inhibitory synapses using immunostaining for gephyrin, an anchoring protein found at the postsynaptic density of GABAergic synapses and involved in the clustering of GABA and glycine receptors (Sassoe-Pognetto and Fritschy 2000). Immunostaining for gephyrin revealed discrete immunoreactive puncta that could be visually identified and quantified (Fig. 9*A*). Prior to P7, layer Ia could not be delineated (Fig. 7*A*) nor did we detect gephyrin expression (data not shown). We thus restricted our analysis to P7, P14, and P60. The density of gephyrin-positive puncta increased significantly with age, from 17.44 ± 1.19 puncta/100 μm^2 at P7 to 26.58 ± 1.07 puncta/100 μm^2 at P60 ($F_{2,8} = 13.87$, $P = 0.0025$, Fig. 9*B*). This increase progressed late into development, as the density of inhibitory synapses was significantly higher at

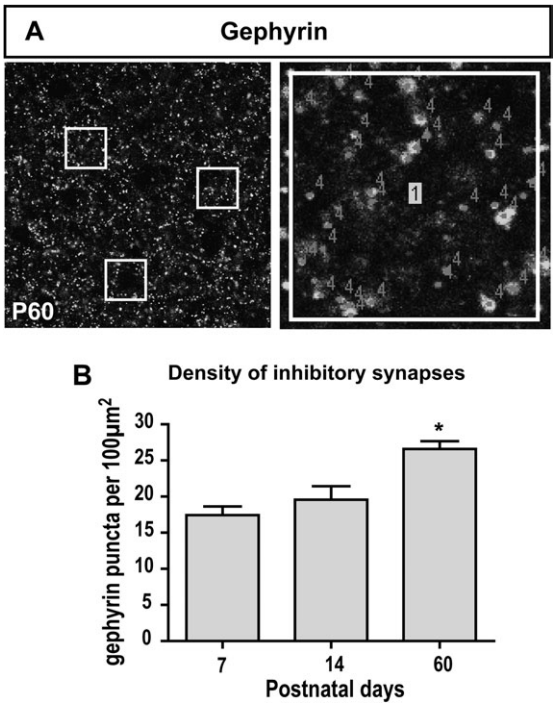

Figure 9. Postnatal changes in inhibitory synapse density. (*A*) Inhibitory synapses in layer Ia were visualized by immunostaining for gephyrin (e.g., at P60). Three regions of interest were selected to count gephyrin-positive puncta. (*B*) Density of gephyrin-positive puncta (labeled "4") in layer Ia per 100 μm^2. Scale bars = 20 μm in *A*1, 2 μm in *A*2. n = 3–4 animals per age. One-way ANOVA followed by Tuckey's post hoc tests. *$P < 0.05$.

P60 than at P7 or P14 ($P < 0.05$). Our data thus show that the density of inhibitory synapses increases relatively late during postnatal development between P14 and P60.

Discussion

Here, we identified pivotal developmental changes that contribute to the postnatal maturation of the aPC with regard to the kinetics of pyramidal cell molecular differentiation, the establishment of cortical lamination, and the maturation of the inhibitory network. These data have broad implications for understanding odor processing in the early postnatal PCX, as well as understanding the ontogeny of trilaminar paleocortices.

Development of the aPC Parallels Neocortical Development

Neurogenesis extends from E11 to E17 in the mouse neocortex (for review, see Molyneaux et al. 2007). Pyramidal neurons are generated in the ventricular and subventricular zones and migrate radially to their final laminar position in the cerebral cortex. Genesis and migration occur in an inside-out distribution based on a cell's date of birth such that late-born neurons migrate past early-born neurons (Angevine and Sidman 1961; Molyneaux et al. 2007; Rakic 2009). In contrast, GABAergic interneurons are a very heterogeneous population; they are generated in the ganglionic eminences during the latter portion of the neurogenic phase (E13.5–E15.5) and migrate tangentially to their ultimate position in the neocortex (for reviews, see Marin and Rubenstein 2001; Wonders and Anderson 2006). Glial cells are born around E18–E19, concomitantly with the end of neurogenesis (Voigt 1989; Culican et al. 1990; Levers et al. 2001). Previous developmental work in PCX suggested similarities to neocortical development. Injections of [^{3}H]thymidine in E14–E22 timed-pregnant rats revealed that significantly more early-born cells settle in layer III as opposed to layer II, reminiscent of the inside-out development of the neocortex (Bayer 1986; Valverde and Santacana 1994). By combining, for the first time, specific molecular markers that enabled us to definitively identify populations of cells, with our BrdU analyses to establish birth-date, we provide here a new perspective on these data. We demonstrate that cell birth-date significantly affects not only the laminar position of cells but also their cellular fate (Fig. 1): 1) a significantly greater proportion of layer II cells are born at E12 than at either E14 or E16 and 2) a large majority of early-born cells (E12 and E14) preferentially differentiate into pyramidal neurons while late-born cells (E16) differentiate into either non-pyramidal neurons (presumably interneurons) or non-neuronal cells (presumably glia). Our results showing the sequential generation of pyramidal cells, interneurons, and glia in the aPC demonstrate the conservation of a fundamental developmental chronology in both paleo- and neocortex.

Molecular Differentiation of Pyramidal Cells

Kinetics of the Molecular Differentiation

Although there has been a focus on the synaptic connectivity of the PCX pyramidal cells and their role in odor processing, little attention has been paid to their molecular differentiation. Englund et al. (2005) describe for the neocortex the sequential expression of 3 transcription factors in the differentiation of radial glia to intermediate progenitor cells to postmitotic pyramidal cells: Pax6 → Tbr2 → Tbr1. This sequence is observed in the embryonic cerebral cortex, adult dentate gyrus, and developing cerebellum, suggesting that it is conserved across cortical regions during both embryonic and adult neurogenesis (for review, see Hevner 2006). Although the role of radial glia as a scaffold for neuronal migration is well understood (for review, see Rakic 2003), their potential role as neuronal precursors is not as well defined (Fishell and Kriegstein 2003; Anthony et al. 2004; Englund et al. 2005). In the E15.5 rat neocortex, transient coexpression of BLBP and the neuronal marker 5A5/E-NCAM has been described in radial glia, suggesting that these cells give rise to glutamatergic neuronal cells (Li et al. 2004). Our results suggest that some radial glia give rise to E16-born pyramidal cells in the aPC by down-regulating expression of BLBP before expressing Tbr1 (Fig. 5).

Our analysis of the molecular differentiation of pyramidal cells in the aPC identified a subset of pyramidal cells that postnatally expressed Tbr1 but not NeuN (Fig. 2*A*). These pyramidal cells were most abundant at P0 but disappeared after P14 (Fig. 2*B*). The loss of Tbr1$^+$NeuN$^-$ cells is unlikely to result from cell death because we did not observe a significant number of apoptotic cells (stained for activated caspase 3) in the aPC at any postnatal ages examined (data not shown). Similarly, only limited cell death was previously reported in the postnatal PCX and neocortex (Friedman and Price 1986; Hevner et al. 2004). Our data thus support the alternative hypothesis that differentiating pyramidal cells successively express Tbr1 and then NeuN. The majority of the pyramidal

cells are molecularly differentiated by P7 in mice, in parallel with their morphological maturation which is almost adult-like by P8 in the rat PCX (Valverde and Santacana 1994). Interestingly, 100% of $Tbr1^+$ postmitotic pyramidal cells already coexpress NeuN in the embryonic neocortex (Englund et al. 2005), suggesting that the kinetics of molecular differentiation of pyramidal cells is slower in the aPC than in the neocortex.

Mechanisms Regulating the Kinetics of Molecular Differentiation

To identify the time required for aPC pyramidal cells to express Tbr1 and NeuN, we examined the sequential expression of these neuronal markers in cells born at E12, E14, and E16. For each population of cells, we determined the approximate number of days after cell birth required for half of the pyramidal cells to express the marker of interest (either Tbr1 alone or both Tbr1 and NeuN) to the time required for all the pyramidal cells to express these makers (Fig. 10). Interestingly, we found that the later-born E16 pyramidal cells required more time than the earlier-born E12 and E14 cells to express both Tbr1 and NeuN from the day of cell birth. For the E12 and E14-born cells, the majority of which were $Tbr1^+NeuN^+$ by P0, the time frame for coexpression of Tbr1 and NeuN was similar, <7–14 days and 5–12 days, respectively (Fig. 10*A–B*). However, E16-born cells required 10–17 days to express Tbr1 alone and 13–24 days to coexpress Tbr1 and NeuN (Fig. 10*C*). These data suggest that the kinetics of Tbr1 and NeuN expression depends on the cell birth-date, with early-born pyramidal cells (E12 and E14) differentiating more rapidly than late-born E16-pyramidal cells. It is possible that this delay can also be accounted for by the time required for pyramidal cells to migrate from the ventricular or subventricular zones to layer II of the aPC; early-born cells have a shorter distance to migrate than the late-born cells because of the developmental increase in brain volume. In support of this hypothesis, the density of E14- and E16-born cells located in layer II increased between P0 and P7, suggesting that cells are still migrating into layer II during the first postnatal week (Fig. 1*B*). Thus, because late-born cells have a longer distance to travel, the perceived delayed maturation of these cells may result in part because some are still migrating at early postnatal ages.

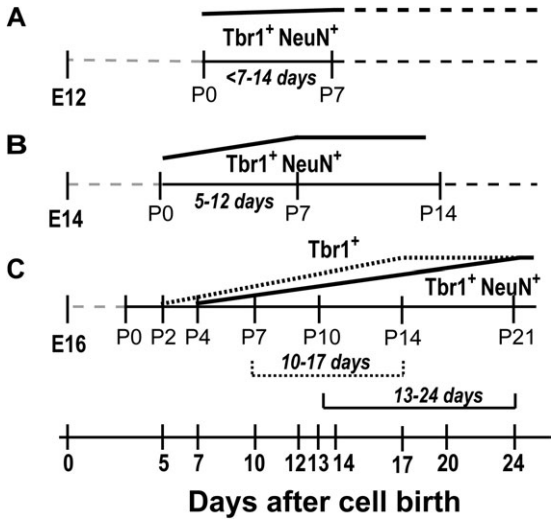

Figure 10. Differential kinetics of pyramidal cell molecular differentiation based on cell birth-date. Schematic summarizing the onset of Tbr1 expression and coexpression of Tbr1 and NeuN by cells born at E12 (*A*), E14 (*B*), and E16 (*C*). Dashed gray lines represent the time period prior to the first analysis (P0), and black dashed lines represent presumed marker expression after the last point of analysis. The dotted line represents expression of Tbr1 only, while solid black lines represent coexpression of Tbr1 and NeuN. For each marker, the range of days represents the day at which approximately half of the pyramidal cells expressed the marker to the earliest point of maximal expression (e.g., 5–12 days for coexpression of Tbr1 and NeuN by E14-born cells).

Finally, close examination of the position of immature versus mature pyramidal cells within layer II suggested that the most superficially located pyramidal cells differentiate more quickly and revealed that immature pyramidal cells are preferentially distributed in the deeper portions of layer II at P0 and P7 (Fig. 2*C–D*). These superficial layer II cells could correspond to the semilunar cells, known to be located in the superficial-most aspect of layer II, and which exhibit firing properties and functions distinct from those of pyramidal cells (Haberly and Behan 1983; Neville and Haberly 2004; Suzuki and Bekkers 2006). It is very likely that semilunar cells express Tbr1, since we did not identify a population of $Tbr1^-NeuN^+$ cells in the superficial-most aspect of layer II (Fig. 2*A*). Our results thus suggest that semilunar cells have a distinct and more accelerated maturation than other pyramidal cells in layer II. Unlike pyramidal cells, semilunar cells lack basal dendrites and the spines of their apical dendrites are concentrated mainly in layer Ia, suggesting that their development could be more heavily influenced by afferent input than the more deeply located pyramidal cells (Heimer and Kalil 1978; Wilson et al. 2000).

Immature $Tbr1^+NeuN^-$ pyramidal cells preferentially resided in the deeper half of layer II at both P0 and P7, but this distribution pattern was more pronounced at P7 than at P0 (Fig. 2). This suggests that immature pyramidal cells are initially uniformly distributed within layer II and that the kinetics of further differentiation (i.e., expression of NeuN) is influenced by their position: pyramidal cells located in the deeper portions of layer II require more time to differentiate than those located more superficially. Alternatively, the distribution of pyramidal cells in layer II may follow an "outside-in" pattern whereby later-born cells settle more deeply in layer II than early-born cells, as previously suggested by Bayer (1986). Our finding that E12-born pyramidal cells are homogenously distributed, while E14-born cells tend to settle in the deeper half of layer II supports this hypothesis (Fig. 4). However, if cell birth-date were the only determinant of cell position, we would expect the immature $Tbr1^+NeuN^-$ cell population to be composed primarily of late-born cells. On the contrary, E12-, E14-, and E16-born cells were equally represented among the immature $Tbr1^+NeuN^-$ pyramidal cells (Fig. 4*E*). In addition, even among the evenly distributed E12-born pyramidal cells, the immature $Tbr1^+NeuN^-$ pyramidal cells were preferentially located deeper in layer II, while the mature $Tbr1^+NeuN^+$ pyramidal cells were evenly distributed throughout the layer (Fig. 4). Collectively, our data provide evidence that the delayed molecular differentiation of deep pyramidal cells in layer II is a result of their position rather than birth-date. This delay may result from the greater distance that the apical dendrites of deeply located pyramidal cells must extend in order to receive input in layer I as compared with the more superficial cells of layer II. Indeed, previous studies suggested the importance of afferent input to the survival of pyramidal cells (Friedman and Price 1986;

Capurso et al. 1997; Leung and Wilson 2003; Koliatsos et al. 2004) and the development of semilunar cell dendritic arborization (Wilson et al. 2000), suggesting that afferent input may be critical to pyramidal cell maturation as well.

Postnatal Development of the Laminar Organization of the aPC

To address pyramidal cell differentiation within the overall development of the aPC, we next examined the emergence of the laminar organization of the aPC. We found that the thickness of the entire aPC and its component layers increased postnatally, although each layer had a specific developmental time course (Fig. 7). Afferent and intracortical fibers were heavily intermingled during the first postnatal days, with the distinction between layers Ia and Ib only emerging at P7 in mouse, similar to previous descriptions in rat (Schwob and Price 1984b; Valverde and Santacana 1994). In addition, while the full thickness of layer I was established early, afferent input via the LOT continued to mature late into postnatal development, extending the temporal framework of layer Ia development.

An increase in the thickness of the LOT likely results from 3 synchronous events: 1) increase in axon diameter (Westrum 1975), 2) increase in axonal branching (Price and Sprich 1975; Devor 1976; Gracey and Scholfield 1990; Walz et al. 2006), and 3) myelination (Westrum 1975; Moriizumi et al. 1995). LOT axons spread across the aPC surface and branch numerous collaterals in the LOT before reaching layer Ia (Devor 1976; Walz et al. 2006). The myelination process extends from ~P10 until the end of the first postnatal month, with the most rapid expansion occurring between P10 and P15 (Moriizumi et al. 1995), paralleling the time course of changes in LOT thickness we report here. LOT axon branching and myelination, along with the ramification of pyramidal cell dendrites, likely contribute to the increase in layer I thickness. In accord with the relatively late development of the thickness of layer Ia, synaptogenesis in this layer is still incomplete by P10, with only 37% of adult synapse density established by this age (Kunkel et al. 1987; Moriizumi et al. 1995).

Development of Inhibitory Mechanisms

GABAergic interneurons are present in all layers of the aPC, where they modulate the activity of pyramidal cells and contribute to odor coding (Loscher et al. 1998; Luna and Schoppa 2008; Poo and Isaacson 2009; Gavrilovici et al. 2010; Luna and Pettit 2010; Suzuki and Bekkers 2010a, 2010b). Different subpopulations of GABAergic interneurons expressing specific molecular markers (calbindin, parvalbumin, vasoactive intestinal protein, somatostatin, or combinations of these) coexist in the adult aPC and display very distinct laminar distributions (Young and Sun 2009; Gavrilovici et al. 2010; Suzuki and Bekkers 2010a, 2010b). There appear to be relatively few interneuron subtypes in the aPC as compared with the neocortex and hippocampus (Suzuki and Bekkers 2010b). We used GAD67-GFP mice to track GABAergic interneurons during postnatal development since a previous study reported that 96% of GABAergic cells in the posterior PCX were GAD67-GFP$^+$ (Young and Sun 2009). Our results provide the first demonstration that the number of GAD67-GFP$^+$ cells decrease during the first postnatal week in the aPC, resulting in a significant decrease of the ratio of interneurons to pyramidal cells (Fig. 8). Since this decrease is observed in all aPC layers, it likely affects all the interneuron subpopulations, although it is possible that each subpopulation follows a distinct evolution.

GAD67-GFP$^+$ cells in the LOT are likely guidepost cells, which are transiently present to guide LOT axons (Sato et al. 1998; Tomioka et al. 2000). However, the decrease in the number of GAD67-GFP$^+$ cells in layers I and II was unexpected. We did not observe massive cell death in the postnatal aPC as assessed with staining against activated caspase-3 (data not shown), strongly suggesting that apoptotic cell death is an unlikely explanation for the disappearance of aPC interneurons after the first postnatal week. This is in agreement with data from the mouse neocortex reporting that cell death is not a significant phenomenon during the first postnatal week, affecting <0.1% of cells, none of which were interneurons (Hevner et al. 2004). Instead, interneurons generated between E13.5 and E16.5 are found to migrate inwardly between P0.5 and P7.5, resulting in a change in laminar position from the marginal zone to the cortical plate (Hevner et al. 2004). As in neocortex (Anderson et al. 1997; Lavdas et al. 1999), GABAergic interneurons located in the PCX originate from the ganglionic eminences (mainly the caudal and medial divisions) (Wichterle et al. 2001; Nery et al. 2002) and migrate over long distances to reach their final destination (Marin and Rubenstein 2001; Ang et al. 2003). It is therefore likely that many of the interneurons present in the aPC between P0 and P4 are migrating to an ultimate position in either layer III, the posterior PCX, or another cortical region. The percentages of both E12- and E14-born interneurons decrease over the first postnatal week (Fig. 6), suggesting that these early-born interneurons are migrating out of aPC and are responsible for the decrease in the total number of interneurons observed in layers I and II during the first postnatal week. This migration flux, in concert with an increase in the area of layer II, might also be responsible for the decreased density of the total E12-born cells between P0 and P7 (Fig. 1*B*).

As shown previously, cortical inhibition matures over the first 3 postnatal weeks in the rat PCX (Schwob, Haberly, and Price 1984). Similarly, GABAergic inhibition in the neocortex progressively develops over the first postnatal month (e.g., Luhmann and Prince 1991; Huang 2009; Okaty et al. 2009), suggesting that the late development of inhibitory mechanisms is a general feature of cortical circuitry. We investigated the morphological basis of the increased inhibition in the postnatal aPC, postulating that the density of inhibitory synapses would increase over the first postnatal weeks. Before the number of interneurons stabilized (P7), we were unable to detect any gephyrin staining and inhibitory synapses in layer Ia, in accordance with previous ultrastructural analysis in rat PCX (Westenbroek et al. 1988). The density of gephyrin-positive puncta in layer Ia then increased between P7 and P60 (Fig. 9). The late increase in inhibitory synapse density (between P14 and P60) parallels the progressive synaptogenesis in layer Ia (Kunkel et al. 1987; Moriizumi et al. 1995) and the late development of mature inhibition in the PCX reported by electrophysiology studies (Schwob, Haberly, and Price 1984).

In aggregate, these data demonstrate that many of the interneurons in the early postnatal aPC make few if any synaptic connections and that the number of inhibitory connections continues to increase relatively late into postnatal development. Thus, we show here that as the interneurons

mature throughout the first postnatal month, they form an increasing number of synaptic connections, as suggested previously in rat (Westenbroek et al. 1988). In conclusion, our data demonstrate that the postnatal maturation of the inhibitory network in the aPC does not proceed through an addition of GABAergic interneurons but rather via an increased density of inhibitory synapses.

Here, we highlighted numerous postnatal events that shape the aPC. The pyramidal cells in layer II differentiate over the first 2 postnatal weeks, sequentially expressing Tbr1 and then NeuN. Late-born cells display delayed maturation, as do cells residing in the deeper aspects of layer II. Late postnatal maturation of the aPC is characterized by reduction in the number of GABAergic interneurons, while there is a compensatory increase in inhibitory synapse density. While the development of the aPC parallels that of the neocortex, our observations suggest that this is a unique structure, especially regarding the development of pyramidal cells. Further study of the specific developmental events that distinguish this 3-layered cortex from 6-layered cortex is necessary, especially given recent interest in the PCX as a general model for cortical sensory processing.

Funding

National Institutes of Health (NIH-NIA-PO1-AG028054 to C.A.G.) and the Richard K. Gershon Yale M.D. student research fellowship to A.A.S.

Notes

We thank D. Montoya and C. Kaliszewski for technical help and members of the Greer laboratory for discussions. *Conflict of Interest*: None declared.

References

Anderson SA, Eisenstat DD, Shi L, Rubenstein JL. 1997. Interneuron migration from basal forebrain to neocortex: dependence on Dlx genes. Science. 278:474–476.

Ang ES, Jr., Haydar TF, Gluncic V, Rakic P. 2003. Four-dimensional migratory coordinates of GABAergic interneurons in the developing mouse cortex. J Neurosci. 23:5805–5815.

Angevine JB, Jr., Sidman RL. 1961. Autoradiographic study of cell migration during histogenesis of cerebral cortex in the mouse. Nature. 192:766–768.

Anthony TE, Klein C, Fishell G, Heintz N. 2004. Radial glia serve as neuronal progenitors in all regions of the central nervous system. Neuron. 41:881–890.

Bayer SA. 1986. Neurogenesis in the rat primary olfactory cortex. Int J Dev Neurosci. 4:251–271.

Bernhardt R, Matus A. 1984. Light and electron microscopic studies of the distribution of microtubule-associated protein 2 in rat brain: a difference between dendritic and axonal cytoskeletons. J Comp Neurol. 226:203–221.

Bulfone A, Wang F, Hevner R, Anderson S, Cutforth T, Chen S, Meneses J, Pedersen R, Axel R, Rubenstein JL. 1998. An olfactory sensory map develops in the absence of normal projection neurons or GABAergic interneurons. Neuron. 21:1273–1282.

Caceres A, Payne MR, Binder LI, Steward O. 1983. Immunocytochemical localization of actin and microtubule-associated protein MAP2 in dendritic spines. Proc Natl Acad Sci U S A. 80:1738–1742.

Capurso SA, Calhoun ME, Sukhov RR, Mouton PR, Price DL, Koliatsos VE. 1997. Deafferentation causes apoptosis in cortical sensory neurons in the adult rat. J Neurosci. 17:7372–7384.

Culican SM, Baumrind NL, Yamamoto M, Pearlman AL. 1990. Cortical radial glia: identification in tissue culture and evidence for their transformation to astrocytes. J Neurosci. 10:684–692.

Devor M. 1976. Fiber trajectories of olfactory bulb efferents in the hamster. J Comp Neurol. 166:31–47.

Englund C, Fink A, Lau C, Pham D, Daza RA, Bulfone A, Kowalczyk T, Hevner RF. 2005. Pax6, Tbr2, and Tbr1 are expressed sequentially by radial glia, intermediate progenitor cells, and postmitotic neurons in developing neocortex. J Neurosci. 25:247–251.

Feng L, Hatten ME, Heintz N. 1994. Brain lipid-binding protein (BLBP): a novel signaling system in the developing mammalian CNS. Neuron. 12:895–908.

Fishell G, Kriegstein AR. 2003. Neurons from radial glia: the consequences of asymmetric inheritance. Curr Opin Neurobiol. 13:34–41.

Friedman B, Price JL. 1986. Age-dependent cell death in the olfactory cortex: lack of transneuronal degeneration in neonates. J Comp Neurol. 246:20–31.

Gavrilovici C, D'Alfonso S, Poulter MO. 2010. Diverse interneuron populations have highly specific interconnectivity in the rat piriform cortex. J Comp Neurol. 518:1570–1588.

Gracey A, Scholfield CN. 1990. Studies on unmyelinated axons and varicosities in the olfactory cortex. Exp Brain Res. 80:436–440.

Haberly L, Behan M. 1983. Structure of the piriform cortex of the opossum. III. Ultrastructural characterization of synaptic terminals of association and olfactory bulb afferent fibers. J Comp Neurol. 219:448–460.

Hartfuss E, Galli R, Heins N, Gotz M. 2001. Characterization of CNS precursor subtypes and radial glia. Dev Biol. 229:15–30.

Heimer L, Kalil R. 1978. Rapid transneuronal degeneration and death of cortical neurons following removal of the olfactory bulb in adult rats. J Comp Neurol. 178:559–609.

Hevner RF. 2006. From radial glia to pyramidal-projection neuron: transcription factor cascades in cerebral cortex development. Mol Neurobiol. 33:33–50.

Hevner RF, Daza RA, Englund C, Kohtz J, Fink A. 2004. Postnatal shifts of interneuron position in the neocortex of normal and reeler mice: evidence for inward radial migration. Neuroscience. 124:605–618.

Huang ZJ. 2009. Activity-dependent development of inhibitory synapses and innervation pattern: role of GABA signalling and beyond. J Physiol. 587:1881–1888.

Illig KR. 2007. Developmental changes in odor-evoked activity in rat piriform cortex. Neuroscience. 145:370–376.

Koliatsos VE, Dawson TM, Kecojevic A, Zhou Y, Wang YF, Huang KX. 2004. Cortical interneurons become activated by deafferentation and instruct the apoptosis of pyramidal neurons. Proc Natl Acad Sci U S A. 101:14264–14269.

Kunkel DD, Westrum LE, Bakay RA. 1987. Primordial synaptic structures and synaptogenesis in rat olfactory cortex. Synapse. 1:191–201.

Lavdas AA, Grigoriou M, Pachnis V, Parnavelas JG. 1999. The medial ganglionic eminence gives rise to a population of early neurons in the developing cerebral cortex. J Neurosci. 19:7881–7888.

Leung CH, Wilson DA. 2003. Trans-neuronal regulation of cortical apoptosis in the adult rat olfactory system. Brain Res. 984:182–188.

Levers TE, Edgar JM, Price DJ. 2001. The fates of cells generated at the end of neurogenesis in developing mouse cortex. J Neurobiol. 48:265–277.

Li H, Babiarz J, Woodbury J, Kane-Goldsmith N, Grumet M. 2004. Spatiotemporal heterogeneity of CNS radial glial cells and their transition to restricted precursors. Dev Biol. 271:225–238.

Loscher W, Lehmann H, Ebert U. 1998. Differences in the distribution of GABA- and GAD-immunoreactive neurons in the anterior and posterior piriform cortex of rats. Brain Res. 800:21–31.

Luhmann HJ, Prince DA. 1991. Postnatal maturation of the GABAergic system in rat neocortex. J Neurophysiol. 65:247–263.

Luna VM, Pettit DL. 2010. Asymmetric rostro-caudal inhibition in the primary olfactory cortex. Nat Neurosci. 13:533–535.

Luna VM, Schoppa NE. 2008. GABAergic circuits control input-spike coupling in the piriform cortex. J Neurosci. 28:8851–8859.

Marin O, Rubenstein JL. 2001. A long, remarkable journey: tangential migration in the telencephalon. Nat Rev Neurosci. 2:780–790.

Molyneaux BJ, Arlotta P, Menezes JR, Macklis JD. 2007. Neuronal subtype specification in the cerebral cortex. Nat Rev Neurosci. 8:427–437.
Moriizumi T, Sakashita H, Furukawa M, Kawano J, Okoyama S, Kitao Y, Kudo M. 1995. Electron microscopic study of synaptogenesis and myelination of the olfactory centers in developing rats. Exp Brain Res. 103:385–392.
Mullen RJ, Buck CR, Smith AM. 1992. NeuN, a neuronal specific nuclear protein in vertebrates. Development. 116:201–211.
Nery S, Fishell G, Corbin JG. 2002. The caudal ganglionic eminence is a source of distinct cortical and subcortical cell populations. Nat Neurosci. 5:1279–1287.
Neville KR, Haberly L. 2004. Olfactory cortex. In: Shepherd GM, editor. The synaptic organization of the brain. 5th ed. New York: Oxford University Press.
Okaty BW, Miller MN, Sugino K, Hempel CM, Nelson SB. 2009. Transcriptional and electrophysiological maturation of neocortical fast-spiking GABAergic interneurons. J Neurosci. 29:7040–7052.
Poo C, Isaacson JS. 2009. Odor representations in olfactory cortex: "sparse" coding, global inhibition, and oscillations. Neuron. 62:850–861.
Price JL. 1973. An autoradiographic study of complementary laminar patterns of termination of afferent fibers to the olfactory cortex. J Comp Neurol. 150:87–108.
Price JL, Sprich WW. 1975. Observations on the lateral olfactory tract of the rat. J Comp Neurol. 162:321–336.
Rakic P. 2003. Elusive radial glial cells: historical and evolutionary perspective. Glia. 43:19–32.
Rakic P. 2009. Evolution of the neocortex: a perspective from developmental biology. Nat Rev Neurosci. 10:724–735.
Sassoe-Pognetto M, Fritschy JM. 2000. Mini-review: gephyrin, a major postsynaptic protein of GABAergic synapses. Eur J Neurosci. 12:2205–2210.
Sato Y, Hirata T, Ogawa M, Fujisawa H. 1998. Requirement for early-generated neurons recognized by monoclonal antibody lot1 in the formation of lateral olfactory tract. J Neurosci. 18:7800–7810.
Schwob JE, Haberly LB, Price JL. 1984. The development of physiological responses of the piriform cortex in rats to stimulation of the lateral olfactory tract. J Comp Neurol. 223:223–237.
Schwob JE, Price JL. 1984a. The development of axonal connections in the central olfactory system of rats. J Comp Neurol. 223:177–202.
Schwob JE, Price JL. 1984b. The development of lamination of afferent fibers to the olfactory cortex in rats, with additional observations in the adult. J Comp Neurol. 223:203–222.
Suzuki N, Bekkers JM. 2006. Neural coding by two classes of principal cells in the mouse piriform cortex. J Neurosci. 26: 11938–11947.
Suzuki N, Bekkers JM. 2010a. Distinctive classes of GABAergic interneurons provide layer-specific phasic inhibition in the anterior piriform cortex. Cereb Cortex.
Suzuki N, Bekkers JM. 2010b. Inhibitory neurons in the anterior piriform cortex of the mouse: classification using molecular markers. J Comp Neurol. 518:1670–1687.
Tamamaki N, Yanagawa Y, Tomioka R, Miyazaki J, Obata K, Kaneko T. 2003. Green fluorescent protein expression and colocalization with calretinin, parvalbumin, and somatostatin in the GAD67-GFP knock-in mouse. J Comp Neurol. 467:60–79.
Tomioka N, Osumi N, Sato Y, Inoue T, Nakamura S, Fujisawa H, Hirata T. 2000. Neocortical origin and tangential migration of guidepost neurons in the lateral olfactory tract. J Neurosci. 20:5802–5812.
Valverde F, Santacana M. 1994. Development and early postnatal maturation of the primary olfactory cortex. Brain Res Dev Brain Res. 80:96–114.
Voigt T. 1989. Development of glial cells in the cerebral wall of ferrets: direct tracing of their transformation from radial glia into astrocytes. J Comp Neurol. 289:74–88.
Walz A, Omura M, Mombaerts P. 2006. Development and topography of the lateral olfactory tract in the mouse: imaging by genetically encoded and injected fluorescent markers. J Neurobiol. 66:835–846.
Westenbroek RE, Westrum LE, Hendrickson AE, Wu JY. 1988. Ultrastructural localization of immunoreactivity in the developing piriform cortex. J Comp Neurol. 274:319–333.
Westrum LE. 1975. Electron microscopy of synaptic structures in olfactory cortex of early postnatal rats. J Neurocytol. 4:713–732.
Wichterle H, Turnbull DH, Nery S, Fishell G, Alvarez-Buylla A. 2001. In utero fate mapping reveals distinct migratory pathways and fates of neurons born in the mammalian basal forebrain. Development. 128:3759–3771.
Wilson DA, Best AR, Brunjes PC. 2000. Trans-neuronal modification of anterior piriform cortical circuitry in the rat. Brain Res. 853: 317–322.
Wonders CP, Anderson SA. 2006. The origin and specification of cortical interneurons. Nat Rev Neurosci. 7:687–696.
Young A, Sun QQ. 2009. GABAergic inhibitory interneurons in the posterior piriform cortex of the GAD67-GFP mouse. Cereb Cortex. 19:3011–3029.